Explicit kernel-split panel-based Nyström schemes for planar or axisymmetric Helmholtz problems

Johan Helsing

Lund University

Talk at "Integral equation methods: fast algorithms and applications", Banff, December 9, 2013

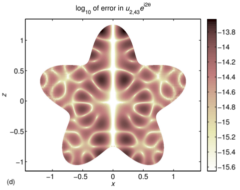

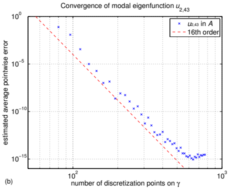

Acknowledgement

The work presented has in part been carried out in cooperation with or been supported by:

- Michael Benedicks
- Björn Dahlberg
- Jonas Englund
- Leslie Greengard
- Bertil Gustafsson
- Anders Karlsson
- Robert V. Kohn
- Graeme Milton
- Gunnar Peters
- Rikard Ojala
- Karl-Mikael Perfekt
- the Swedish Research Council

Outline

Recent trends in my own reserach, which has become (even more) application driven and now focuses on scattering problems

- Helmholtz equation
- Geometries
- Integral equations with split kernels
- Philosophy
- Overview of numerical tools
- Product integration
- Multilevel discretization
- Numerical examples
- Relevance for particle accelerator design

Helmholtz equation

Exterior Dirichlet planar problem

$$\Delta u(r) + k^2 u(r) = 0\,, \quad r \in E$$
$$u(r) = g(r)\,, \quad r \in \gamma$$
$$\lim_{|r|\to\infty} \sqrt{|r|}\left(\frac{\partial}{\partial|r|} - \mathrm{i}k\right) u(r) = 0$$

Interior Neumann axisymmetric problem

$$\Delta u(\mathbf{r}) + k^2 u(\mathbf{r}) = 0\,, \quad \mathbf{r} \in V$$
$$\boldsymbol{\nu} \cdot \nabla u(\mathbf{r}) = f(\mathbf{r})\,, \quad \mathbf{r} \in \Gamma$$

Fourier methods will be used in the azimuthal direction.

Planar problem: geometry

Planar Exterior Helmholtz Dirichlet problem

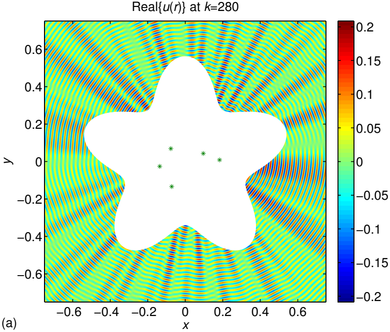

Figure: Setup from Hao, Barnett, Martinsson, and Young, *Adv. Comput. Math.*, (2013, in press).

Axisymmetric problem: geometry

Coordinates for body of revolution

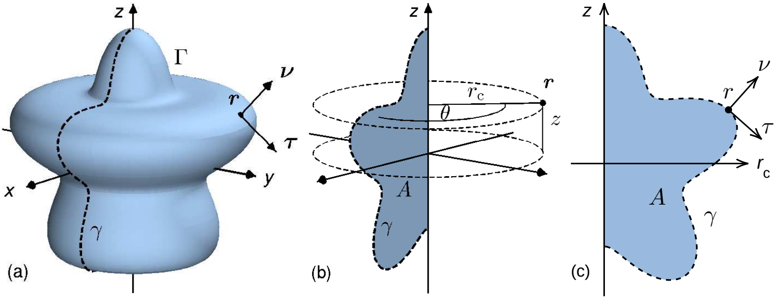

Figure: An axially symmetric surface Γ generated by a curve γ. (a) Unit normal $\boldsymbol{\nu}$ and tangent vector $\boldsymbol{\tau}$. (b) **r** has radial distance r_c, azimuthal angle θ, and height z. The planar domain A is bounded by γ and the z-axis. (c) Coordinate axes and vectors in the half-plane $\theta = 0$.

Planar problem: integral equation

Planar Exterior Helmholtz Dirichlet problem

$$\rho(r)+\int_\gamma K(r,r')\rho(r')\,\mathrm{d}\gamma' - \mathrm{i}\frac{k}{2}\int_\gamma S(r,r')\rho(r')\,\mathrm{d}\gamma' = 2g(r)\,, \quad r\in\gamma$$

where K and S depend on k. Note the coupling parameter.

Splits:

$$S(r,r') = \tilde{G}_1(r,r') - \frac{2}{\pi}\log|r-r'|\Im\{S(r,r')\}$$
$$K(r,r') = \tilde{G}_2(r,r') - \frac{2}{\pi}\log|r-r'|\Im\{K(r,r')\}$$

where $\tilde{G}_1$, $\tilde{G}_2$, $\Im\{S\}$, and $\Im\{K\}$ are smooth functions. Similar for post-processor.

Axisymmetric problem: integral equation

Axisymmetric interior Helmholtz Neumann problem. Modal equations:

$$\rho_n(r) + 2\sqrt{2\pi}\int_\gamma K_n^t(r,r')\rho_n(r')r'_{\mathrm{c}}\,\mathrm{d}\gamma' = 2f_n(r)\,, \quad n = 0,\ldots$$

$$K_n^t(r,r') = \tilde{K}_n^t(r,r') + \frac{1}{\sqrt{2\pi}}\sum_m D_m^t(r,r')\tilde{G}_{3,n-m}(r,r')$$

$$D_n^t(r,r') = \tilde{G}_4(r,r')\mathfrak{Q}_{n-\frac{1}{2}}(\chi) + \tilde{G}_5(r,r')\mathfrak{Q}_{n-\frac{3}{2}}(\chi)$$

$$\chi = 1 + \frac{|r-r'|^2}{2r_{\mathrm{c}}r'_{\mathrm{c}}}$$

Split:

$$\mathfrak{Q}_{n-\frac{1}{2}}(\chi) = -\frac{1}{2}\log(\chi-1)\,{}_2\tilde{F}_1\left(\frac{1}{2}-n, \frac{1}{2}+n; 1; \frac{1-\chi}{2}\right) + \tilde{G}_6(\chi,n)$$

Philosophy

- Automatization
- Computing on-the-fly
- Optimal accuracy
- Discretization economy
- Solutions available everywhere in domain
- Exploitation of known analytical information

Numerical tools

- Nyström scheme with panelwise Gauss–Legendre quadrature
- Fast product integration for (near) singular logarithmic- and Cauchy-type kernels
- Matrix splittings $\mathbf{M} = \mathbf{M}^{\star} + \mathbf{M}^{\circ}$
- Multilevel discretization – coarse and fine grids
- Panelwise interpolation operators $\mathbf{P}$, $\mathbf{Q}$, and $\mathbf{P}_W$.
- Hankel functions $H_n^{(1)}(z)$ and toroidal harmonics $\mathfrak{Q}_{n-\frac{1}{2}}(z)$

Product integration

Given a parameterization $\gamma(t)$, a quadrature t_i, w_i and

$$I_p(r) = \int_{\gamma_p} G(r, r')\rho(r')\,\mathrm{d}\gamma'$$

$$G(r, r') = \tilde{G}_0(r, r') + \log|r - r'|\tilde{G}_{\mathrm{L}}(r, r') + \frac{(r' - r)\cdot\nu'}{|r' - r|^2}\tilde{G}_{\mathrm{C}}(r, r')$$

it holds, on the fly and in practice, to order $n_{\mathrm{pt}} \leq 32$

$$I_p(r) = \sum_{j=1}^{n_{\mathrm{pt}}} G(r, r_j)\rho_j s_j w_j + \sum_{j=1}^{n_{\mathrm{pt}}} \tilde{G}_{\mathrm{L}}(r, r_j)\rho_j s_j w_j w_{\mathrm{L}j}^{\mathrm{corr}}(r)$$
$$+ \sum_{j=1}^{n_{\mathrm{pt}}} \tilde{G}_{\mathrm{C}}(r, r_j)\rho_j w_{\mathrm{C}j}^{\mathrm{cmp}}(r)$$

Variants of schemes

General form of discretized integral equation

$$\left(\mathbf{I} + \mathbf{M}_\gamma^\star + \mathbf{M}_\gamma^\circ\right)\boldsymbol{\rho} = 2\mathbf{g}$$

Post-processor

$$\mathbf{u} = \left(\mathbf{M}_E^\star + \mathbf{M}_E^\circ\right)\boldsymbol{\rho}$$

Abbreviations in what follows

(1) coarse grid on γ

(2) fine grid on γ

(3) field points in the exterior E

Variants of schemes

Scheme A: everything on the coarse grid

$$\left(\mathbf{I}^{(11)} + \mathbf{M}_{\gamma}^{\star(11)} + \mathbf{M}_{\gamma}^{\circ(11)}\right)\boldsymbol{\rho}^{(1)} = 2\mathbf{g}^{(1)}$$

$$\mathbf{u}^{(3)} = \left(\mathbf{M}_{E}^{\star(31)} + \mathbf{M}_{E}^{\circ(31)}\right)\boldsymbol{\rho}^{(1)}$$

Scheme B: close interaction on the fine grid

$$\left(\mathbf{I}^{(11)} + \mathbf{Q}\mathbf{M}_{\gamma}^{\star(22)}\mathbf{P} + \mathbf{M}_{\gamma}^{\circ(11)}\right)\boldsymbol{\rho}^{(1)} = 2\mathbf{g}^{(1)}$$

$$\mathbf{u}^{(3)} = \left(\mathbf{M}_{E}^{\star(32)}\mathbf{P} + \mathbf{M}_{E}^{\star\circ(32)}\mathbf{P} + \mathbf{M}_{E}^{\circ(31)}\right)\boldsymbol{\rho}^{(1)}$$

Scheme C: same as scheme B, but with equal arc length panels

Variants of schemes

Scheme D: more uknknowns, but same work for main matrix-vector multiplications

$$\left(\mathbf{I}^{(22)} + \mathbf{M}_{\gamma}^{\star(22)} + \mathbf{P}\mathbf{M}_{\gamma}^{\circ(11)}\mathbf{P}_W^T\right)\boldsymbol{\rho}^{(2)} = 2\mathbf{g}^{(2)}$$

$$\mathbf{u}^{(3)} = \left(\mathbf{M}_E^{\star(32)} + \mathbf{M}_E^{\star\circ(32)} + \mathbf{M}_E^{\circ(31)}\mathbf{P}_W^T\right)\boldsymbol{\rho}^{(2)}$$

Scheme E: even more dominant role for fine grid in integral equation

$$\left(\mathbf{I}^{(22)} + \mathbf{M}_{\gamma}^{\star(22)} + \mathbf{M}_{\gamma}^{\circ(21)}\mathbf{P}_W^T\right)\boldsymbol{\rho}^{(2)} = 2\mathbf{g}^{(2)}$$

$$\mathbf{u}^{(3)} = \left(\mathbf{M}_E^{\star(32)} + \mathbf{M}_E^{\star\circ(32)} + \mathbf{M}_E^{\circ(31)}\mathbf{P}_W^T\right)\boldsymbol{\rho}^{(2)}$$

Planar problem: results

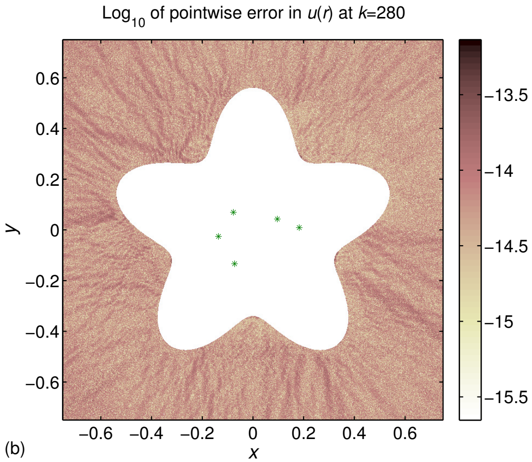

Figure: $\log_{10}$ of pointwise error in $u(r)$, normalized with $\max|u(r)|$, at 347,650 near-field points. Scheme E is used with 140 panels on γ. The sources that generate the boundary conditions appear as green stars.

Planar problem: results

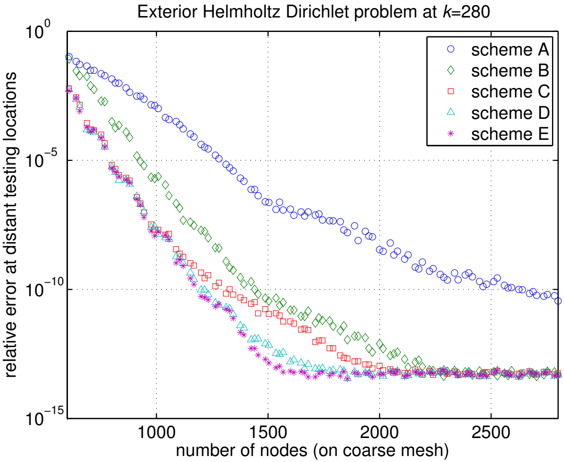

Figure: Far field tests.

Planar problem: results

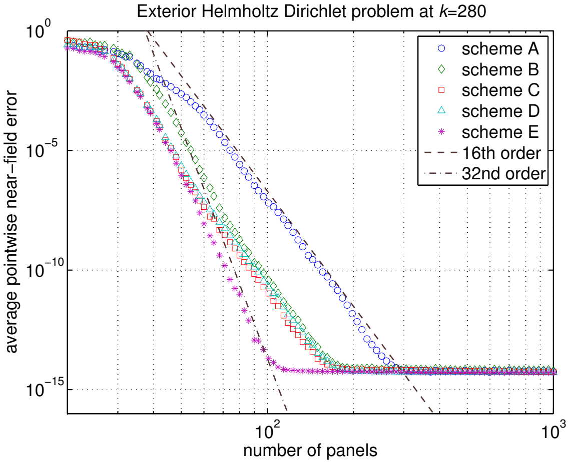

Figure: Near field tests.

Axisymmetric problem: results

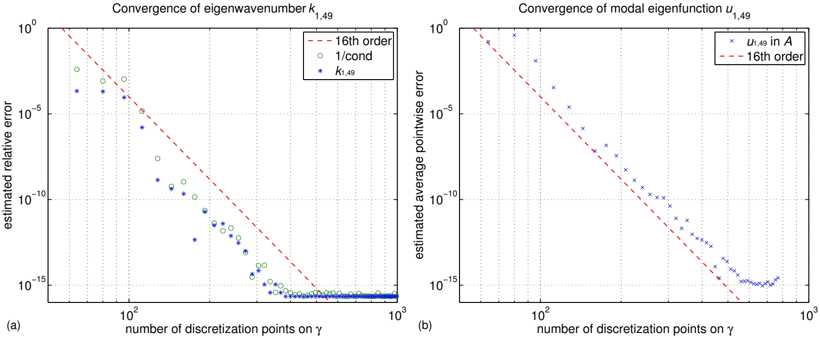

Figure: Convergence of the Laplace Neumann eigenpair $u_{1,49}(r)$ and $k_{1,49} \approx 19.22942004015467$. (a) Reciprocal condition number and error in $k_{1,49}$. (b) Estimated average pointwise error in $u_{1,49}(r)$.

Axisymmetric problem: results

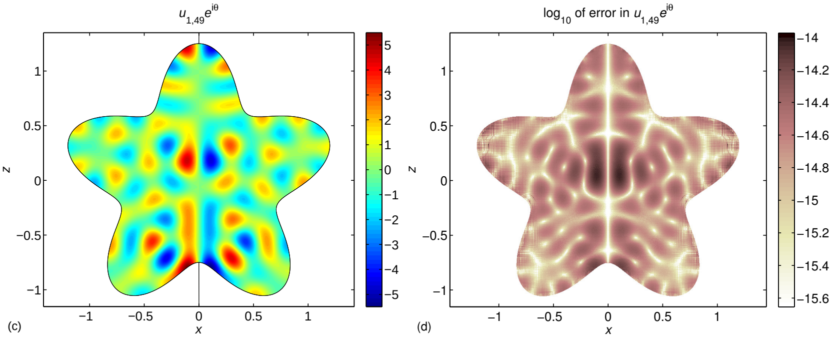

Figure: Normalized Neumann Laplace eigenfunction $u_{1,49}(r)$. (c) The field $u_{1,49}(r)e^{\mathrm{i}\theta}$ for $\theta = 0$ and $\theta = \pi$ with 608 points on γ. (d) $\log_{10}$ of pointwise error in $u_{1,49}(r)e^{\mathrm{i}\theta}$ for $\theta = 0$ and $\theta = \pi$.

Axisymmetric problem: results

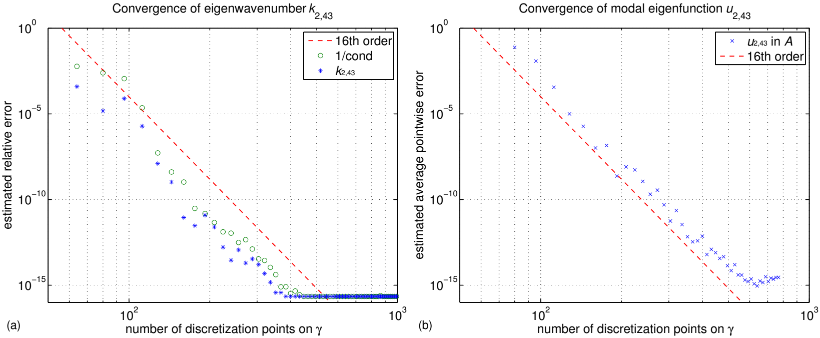

Figure: Convergence of the Laplace Neumann eigenpair $u_{2,43}(r)$ and $k_{2,43} \approx 19.21873987061249$. (a) Reciprocal condition number and error in $k_{2,43}$. (b) Estimated average pointwise error in $u_{2,43}(r)$.

Axisymmetric problem: results

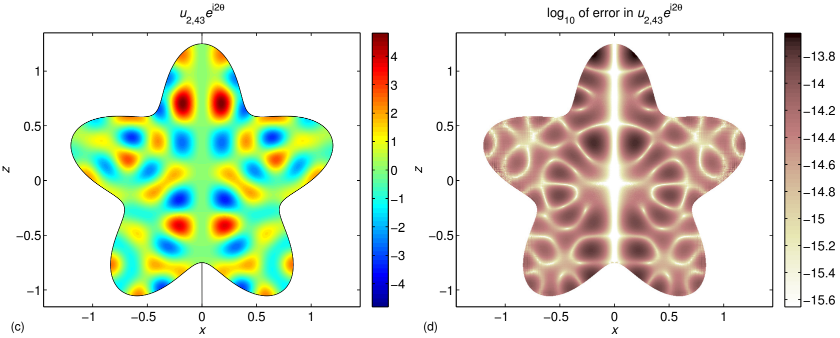

Figure: Normalized Neumann Laplace eigenfunction $u_{2,43}(r)$. (c) The field $u_{2,43}(r)e^{i\theta}$ for $\theta = 0$ and $\theta = \pi$ with 608 points on γ. (d) $\log_{10}$ of pointwise error in $u_{2,43}(r)e^{i\theta}$ for $\theta = 0$ and $\theta = \pi$.

Conclusions

- Explicit kernel-split panel-based Nyström discretization schemes with quadratures computed on the fly seem competitive for planar and axisymmetric BVP.
- Log and Cauchy kernels suffice most of the time.
- Comparing schemes is difficult.
- Fast methods for non-linear eigenvalue problems needed in applications to accelerator design.
- Incorporation of fast direct solvers?

References

- J. Helsing, "Solving integral equations on piecewise smooth boundaries using the RCIP method: a tutorial", *Abstr. Appl. Anal.*, **2013**, Article ID 938167 (2013).
- J. Helsing and A. Holst, "Variants of an explicit kernel-split panel-based Nyström discretization scheme for Helmholtz boundary value problems", `arXiv:1311.6258 [math.NA]` (2013).
- J. Helsing and A. Karlsson, "An accurate solver for boundary value problems applied to the scattering of electromagnetic waves from two-dimensional objects with corners", IEEE Trans. Antennas Propag., **61**, 3693–3700 (2013).
- J. Helsing, "Integral equation methods for elliptic problems with boundary conditions of mixed type", *J. Comput. Phys.*, **228**(23), 8892–8907 (2009).